Received: 16 January 2025 | Revised: 7 March 2025 | Accepted: 30 March 2025

DOI: 10.1002/aic.18853

AIChE JOURNAL

RESEARCH ARTICLE

Biomolecular Engineering

Physics-informed neural networks (PINNs) for high-resolutional prediction of shear stress on cells in suspension culture

Ikki Horiguchi | Keisuke Shima | Yasunori Okano

Division of Chemical Engineering, Graduate School of Engineering Science, Osaka University, Osaka, Japan

Correspondence
Ikki Horiguchi, Division of Chemical Engineering, Graduate School of Engineering Science, Osaka University, 1-3, Machikaneyama-cho, Toyonaka-shi, Osaka, 560-8531, Japan.
Email: horiguchi.ikki.es@osaka-u.ac.jp

Funding information
Japan Society for the Promotion of Science, Grant/Award Number: JP23K04507

Abstract

The effect of shear stress on cell behaviors should be considered for designing the suspension culture of mammalian cells. Computational flow dynamics (CFD) is a promising tool for estimating shear stress on cells, but the accuracy is limited due to resolution limitations. In this research, we applied physics-informed neural networks (PINNs) for the high-resolution estimation of shear and drag stress on the cells in a swirling suspension culture. PINNs could complement the flow in the mesh and estimate the shear and drag stresses on the surface of cell particles smaller than the mesh size. The estimated shear and drag stress was lower than that from CFD calculation, and the shear stress depended on the non-dimensional number such as the Froude number. This approach could solve the limitation of the resolution of CFD for estimation of shear stress on the cells and is helpful to develop the large-scale suspension culture.

KEYWORDS
CFD, PINNs, shear stress, suspension culture

1 | INTRODUCTION

Suspension culture is expected for mass production of mammalian cells. Mammalian cells are widely used for biopharmaceuticals such as regenerative tissue, antibodies, and vaccines. Therefore, various types of mammalian cells are applied to suspension culture. For example, Chinese hamster ovary (CHO) cells are cultured in a suspension bioreactor for producing antibiotic pharmaceuticals, and they are expanded to more than 10^7 cells for industrial application.[1] In other instances, induced pluripotent stem (iPS) cells were cultured in suspension culture with high expectations for the cell source of artificial tissue for regenerative therapy and drug screening.[2] In the case of iPS cell suspension culture, there are two different operations (expansion and differentiation), which complicate suspension culture.

To design suspension culture of some mammalian cells, such as iPS cells, the effect of shear stress is one of the most important factors to be considered. The suspension culture of mammalian cells requires agitation to keep cells floating and distributed and to supply oxygen. The effect of stress from culture medium flow on cell behavior is well-known, and there are many reports about it. Compared to microorganisms, mammalian cells are more sensitive to shear stress and exhibit a variety of responses, including morphological changes,[3,4] cell death,[5–8] and differentiation.[3,9] Therefore, the design of floating suspension culture of mammalian cells requires repeated trials, but the high cost of suspension culture limits the repetition of suspension culture for development. Therefore, estimating shear stress is important for developing and optimizing bioreactors. Recently, various attempts have been demonstrated to estimate shear stress during

suspension culture. As an experimental approach, particle tracking has been proposed as a method to estimate cellular load during suspension culture,[10] but these experimental approaches are still developing.

To estimate the shear stress on the cells in suspension culture, computational fluid dynamics (CFD) is a powerful tool and studied for developing bioreactors for suspension culture. As mentioned above, the experimental strategy requires repeated experiments, which are very time-consuming and costly. In contrast, the CFD approach can save experimental costs and evaluate various conditions simultaneously as computational resources allow. Therefore, there is various CFD research for evaluating bioreactors.[11,12] Most of them have calculated only fluid dynamics, and few have calculated fluid dynamics including actual cellular dynamics as well.[13] This is because of the complexity of coupling CFD, which calculates the behavior of the fluid, and the discrete element method (DEM), which calculates the behavior of the cell particles. In addition, the size of cellular particles (approximately 20 μm diameter and 4 nL volume) is much smaller than that of bioreactors (approximately 0.1–100 L). It means that precise DEM simulation in the bioreactor requires the CFD with high resolution, which requires a huge amount of calculation resources and calculation time.

Machine learning could effectively overcome the resolution limitations of the coupling of CFD/DEM. Machine-learning-supported CFD is being developed as a surrogate model[14] since the development of machine learning, including neural networks. The outputs of these neural networks are continuous and do not require discretization by mesh preparation. Especially, physics informed neural networks (PINNs) can output results that obey the laws of physics by using physical governing equations (e.g., Navier–Stokes equation) for training.[15] Recently, as a demonstration of PINNs, Mahmoudabadbozchelou et al. applied PINNs to estimate the fluid dynamics of a non-Newtonian fluid,[16] and Qiu et al. demonstrated PINNs for two-phase flow.[17] For process development, Takehara et al. applied PINNs for fast prediction of transport phenomena during the crystal growth of silicon.[18] Thus, PINNs have been expected and studied as a surrogate model in recent simulations.

In this research, we utilized PINNs to estimate shear stress on the surface of cells from CFD data. As mentioned above, there is a limitation of the resolution in the CFD approach for cell suspension culture. PINNs are expected to complement the flow in the mesh based on the governing equations of the Navier–Stokes equation and the continuity equation. Estimated flow in the mesh can estimate the velocity gradient on the cells and shear and drag stress. In addition, we also obtained the time profile of shear stress and evaluated the relationship between shear stress and process parameters like the Froude number. Except for the suspension culture, cells are exposed to medium flow during many parts of the culture, not only in suspension culture. For example, nozzle-based suction and ejection operations are widely used in cell culture and bioprinting, but the flow velocity at the nozzle tip is higher, and effects such as cell damage due to shear stress have been pointed out.[19] Thus, the PINNs method is important for designing not only suspension culture but also cell culture operations.

2 | NUMERICAL METHODOLOGIES

2.1 | Model overview

The cylindrical tank with variable diameter (d_t) and height (h_t) is proposed as a swirling bioreactor (Figure 1A). The bioreactor has two phases (air/water), and height of water (h_w) is variable. The bioreactor swirls without spinning around a circular orbit of radius R for the agitation, and its rotational speed (ω) is a variable. In CFD, centrifugal force was applied as an external force term to calculate the liquid flow and particle behavior in the bioreactor as a stationary coordinate system. The centrifugal acceleration (a_c) is applied and defined by Equations 1 and 2.

$$a_c = \frac{d^2 r}{dt^2} \tag{1}$$

$$r = \begin{pmatrix} x \\ y \\ z \end{pmatrix} = \begin{pmatrix} R\cos\omega t \\ -R\sin\omega t \\ 0 \end{pmatrix} \tag{2}$$

In the calculations, the fluid was assumed to be a Newtonian fluid, and no reactions or changes in temperature or physical properties occurred inside the reactor. iPSC aggregates were assumed to be solid particles without any changes in size, shape, and properties. Furthermore, the proportion of particles in the liquid was assumed to be sufficiently small that collisions between particles and forces exerted by particles on the fluid were negligible, and only forces exerted by the fluid on the particles were considered.

2.2 | Computational flow dynamics for cells and medium in swirling culture

OpenFOAM-2.4.x was used for developing and running the solver to calculate the medium flow and particle behavior. The details of the solver are mentioned, and the solver was validated in previous research.[20]

Briefly, we calculated the flow dynamics with liquid/gas interfaces and particle behavior moving in a liquid flow. To calculate fluid velocity and pressure, the Reynolds-averaged continuity equation (Equation 3) and the Navier–Stokes equation (Equation 4) were used as the governing equations.

$$\nabla \cdot v_f = 0 \tag{3}$$

$$\frac{\partial}{\partial t}\rho_f \overline{v_f} + \nabla \cdot (\rho_f \overline{v_f}\,\overline{v_f}) = -\nabla p + \nabla \cdot ((\mu_f + \mu_t)\nabla \overline{v_f}) + \rho_f g - \rho_f a_c + \gamma\kappa\nabla\alpha \tag{4}$$

Here, v is the flow velocity vector, p is pressure, μ is viscosity, and ρ is weight density. Overline on v indicates time-averaged value. Thereafter, the variable's subscript f means fluid, p means particle. The fourth term on the right side in Equation 4 represents the

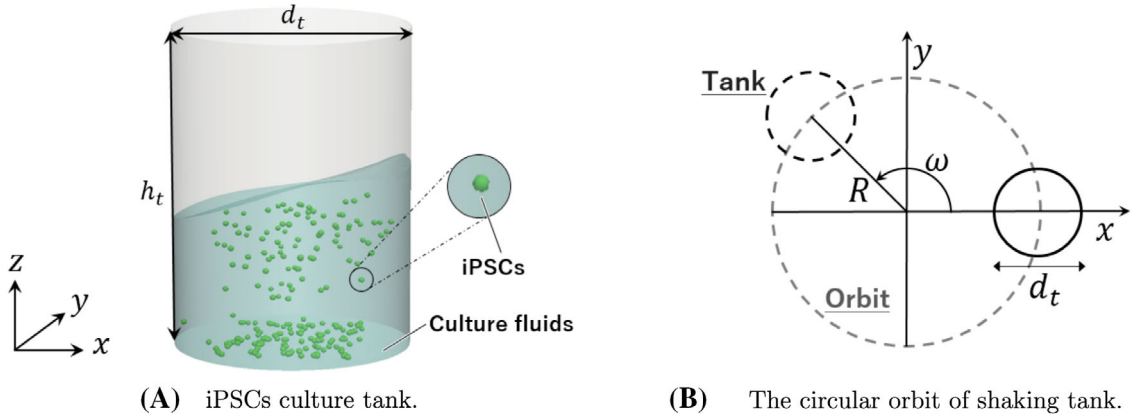

(A) iPSCs culture tank. **(B)** The circular orbit of shaking tank.

FIGURE 1 Geometrical drawing of (A) iPSCs culture tank and (B) orbital shaking culture system.

centrifugal force due to the swirling concussion. The fifth term on the right side in Equation 4 represents the surface tension on the liquid–gas interface, derived by the continuum surface model. κ represents a curvature. To represent the gas–liquid interface, volume of fluid (VOF) method is utilized. To calculate the turbulent flow features, the reliable k–ε turbulence model was employed.

The discrete element method (DEM) was employed to calculate particle behavior. Newton's second equation of motion (Equation 5) was used as the governing equation for solid particles.

$$m_p \frac{dv_p}{dt} = F_d + F_g + F_l + F_{vm} - m_p a_c \tag{5}$$

Here, F_d represents the drag force from liquid, F_g represents buoyancy, F_l represents the lift force created by the pressure gradient around the particles, and F_{vm} represents virtual mass force. The last term on the right side in Equation 5 represents the centrifugal force on the particles. Collision model of particle was not applied because the cell density is low enough that cell–cell collisions can be considered negligible in actual iPSC suspension cultures and the number of particles used in the numerical simulation was significantly lower than in the actual culture systems due to the computational limitations.

The finite volume method (FVM) was employed to discretize the governing equations. The convection term in the transport equation for volume fraction α is determined by second-order precision total variation diminishing (TVD), the convection terms in the transport equation for k and ε are determined by first-order precision upwind differencing, and the other terms are determined by second-order precision central differencing. The first-order precision Euler implicit method was employed for time discretization. The pressure implicit with splitting operator (PISO) method is used to compute velocity and pressure.

Calculation was performed by the Intel(R) Xeon(R) Gold 6338 CPU @ 2.00GHz. The computation time was approximately 17 h.

2.3 | Physics informed neural networks

Physics informed neural networks called PINNs are machine learning technique used to solve nonlinear partial differential equations such as Navier–Stokes equations. The solver was developed and mentioned in previous research.[18] The architecture of PINNs is shown in Figure 2. PINNs are divided into two parts: calculates the error between the predictions at NN and the teacher data, and calculates the error in the governing equations that describe the physical phenomenon. The input vector $\boldsymbol{X}$ of PINNs is shown as $\boldsymbol{X} = (x,y,z,t)$.

Firstly, the prediction target is parameterized to various coordinates and times, and the pressure and velocity distributions are comprehensively predicted. The error between the supervised CFD data and PINNs predictions for each physical quantity is evaluated by the mean squared error shown in Equation 6.

$$L_{CFD} = \frac{1}{N_{CFD}} \sum_{j=1}^{N_{CFD}} \left[\boldsymbol{U}_{pred}(\boldsymbol{X}_j) - \boldsymbol{U}_{CFD}(\boldsymbol{X}_j) \right]^2 \tag{6}$$

$\boldsymbol{U}_{pred}$ and $\boldsymbol{U}_{CFD}$ are the PINNs and CFD analysis results corresponding to the input parameter $\boldsymbol{X}$, and N_{CFD} is the number of points of learned CFD data. Here, the error with the CFD data and the error with B.C. are collectively defined as the "NN error." In general PINNs, CFD data are not used, and only the governing equations and boundary conditions are learned. However, the flow of the system is complex and much time is required for learning. Therefore, the results from CFD are used to perform highly accurate interpolation of this data.

Second, defined the loss of governing equations. The loss in the continuity equation and Navier–Stokes equation is defined as L_g and L_h.

$$L_g = \frac{1}{N} \sum_{j=1}^{N} \left| g(\boldsymbol{X}_j) \right|^2 \tag{7}$$

$$L_h = \frac{1}{N} \sum_{j=1}^{N} \left| h(\boldsymbol{X}_j) \right|^2 \tag{8}$$

where N is the number of teaching data, and the errors in each governing equation are collectively referred to as the PI error.

For the predicted values to be physically meaningful and accurate, the loss of both the NN and PI errors must be minimized. The loss function L_{all} that minimizes PINNs is defined as a linear combination of each valuation index as follow:

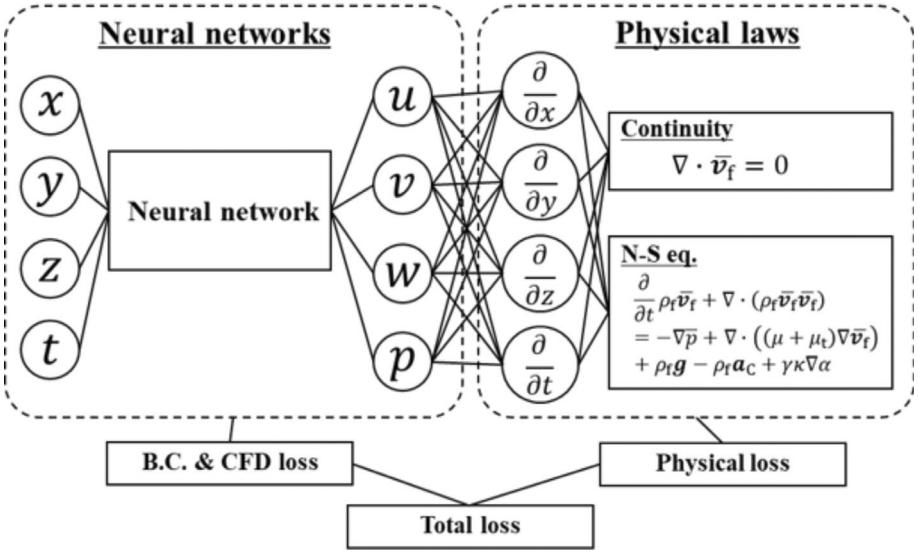

FIGURE 2 Schematic drawing of the PINNs architecture utilized in the manuscript.

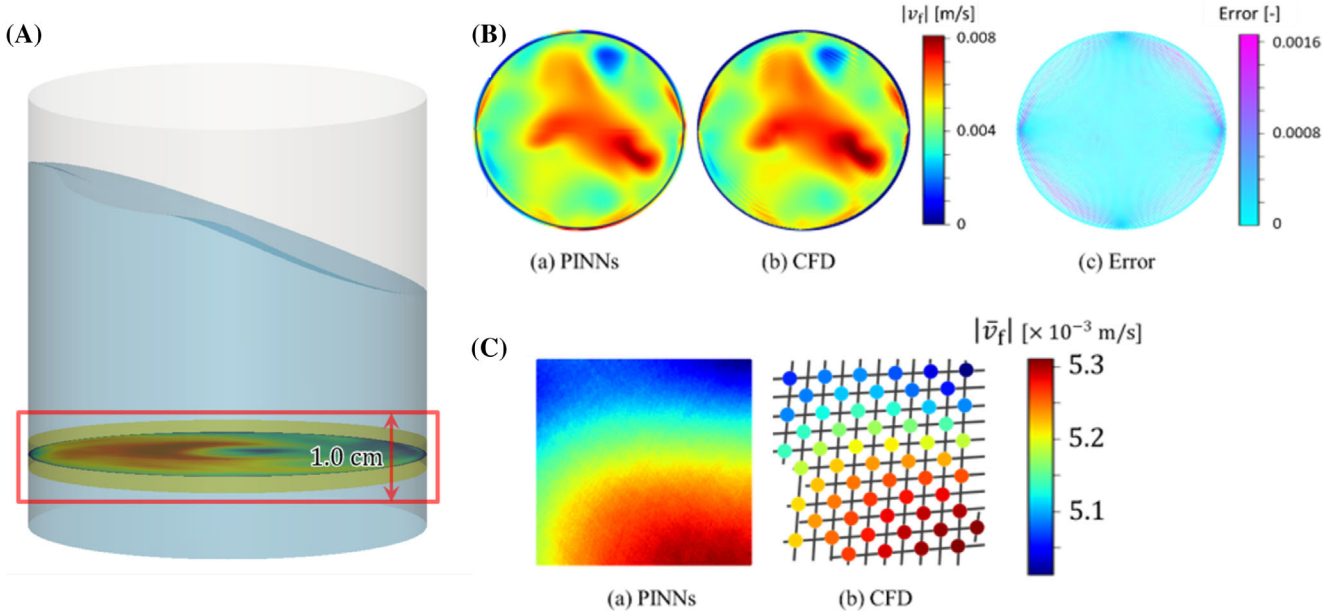

FIGURE 3 (A) Location of calculation data for validation, (B) velocity distribution calculated by PINNs and CFD, and mean squared error between the calculated velocities, and (C) data points of velocity in the small area calculated by PINNs and CFD.

$$L_{\text{all}} = L_{\text{CFD}} + L_g + L_h \tag{9}$$

Although the loss function is defined by adding the NN and PI errors equivalently, they have inherently different physical meanings. In order to examine how much impact each error has on the prediction, a weight parameter is used, and the loss function is as follows:

$$L_{\text{all}} = w_{\text{CFD}} \cdot L_{\text{CFD}} + w_g \cdot L_g + w_h \cdot L_h \tag{10}$$

where w_{CFD}, w_g, w_h are the weight parameters in the error with CFD, the error with continuity equation and the error with Navier–Stokes equation.

Nvidia GeForce RTX 3090 was used for training the neural network, with a training time of approximately 2 h and an execution time of approximately 5 min.

3 | RESULTS AND DISCUSSION

3.1 | PINNs validation

First, we validate the PINNs created in this study by comparing the results obtained by CFD with those predicted by PINNs for the flow at the bottom of the culture medium (shown in Figure 3A). We thinned out the original CFD data at an arbitrary rate and train PINNs

and compare these predicted results with the original data to check for consistency.

Numerical results and PINNs predictions are shown in Figure 3B. PINNs predictions were generally in agreement with the numerical calculations, and the errors between CFD and PINNs were very small except near the wall of the tank. The reason for the large prediction error near the walls is that it is difficult to converge strictly to the no-slip condition. The results in the smaller region of the prediction are shown in Figure 3C. Numerical calculation had a limit to the size of the computational grid, which also limits the resolution of the results obtained. On the other hand, it was possible for PINNs to predict results with higher accuracy even in a small region while performing interpolation. When focusing on smaller regions, the change in the velocity field for each point to be predicted is expected to be smaller, and the change in the Reynolds number is expected to be milder. Here, the predictions can be made at a computational grid ratio of 1/100, and it can be inferred that the predictions in the smaller, milder region are also correct. Therefore, it can be said that the analysis program developed in this study is sufficiently accurate for prediction.

3.2 | Estimation of shear and drag stress on cell particle surface

The PINNs validated in the previous section are used to predict the shear stress and vertical stress on the cell surface. When learning all regions within a container, a huge amount of data is required, making it difficult to make accurate predictions. Therefore, in this study, we focus on a single particle in the container and use the vicinity data of the particle as the learning target. The particle to be selected is the one with the maximum relative velocity between the particle and the fluid at each time step.

The predicted shear and vertical stresses on the surface are shown in Figure 4A,B respectively. This result is a snapshot taken 30 s after the start of stirring, under the stirring condition of $(\omega, R) =$ (90 rpm, 1.5 cm). In this prediction, the distribution over the cell surface was obtained, which was difficult to predict by CFD due to the cell particles were smaller than the mesh. The points on the surface with the highest shear and vertical stresses are indicated by star points. The predictions can account for large localized forces acting on the cell surface. The following discussion will use the maximum values on each surface.

Next, we compare the prediction results of the two methods, CFD and PINNs. The time evolution of the shear stress for each method is shown in Figure 4C under the stirring conditions of $(\omega, R) = (90\,\text{rpm}, 1.5\,\text{cm})$ from 20 to 30 s after the start of stirring. This shows that the calculated shear stress values for CFD and PINNs are significantly different from each other. This can be attributed to two factors. First, the differentiation methods are different. CFD uses a finite volume discretization method, whereas PINNs uses automatic differentiation with backpropagation. In numerical differentiation, it is difficult to account for higher-order differential coefficients because

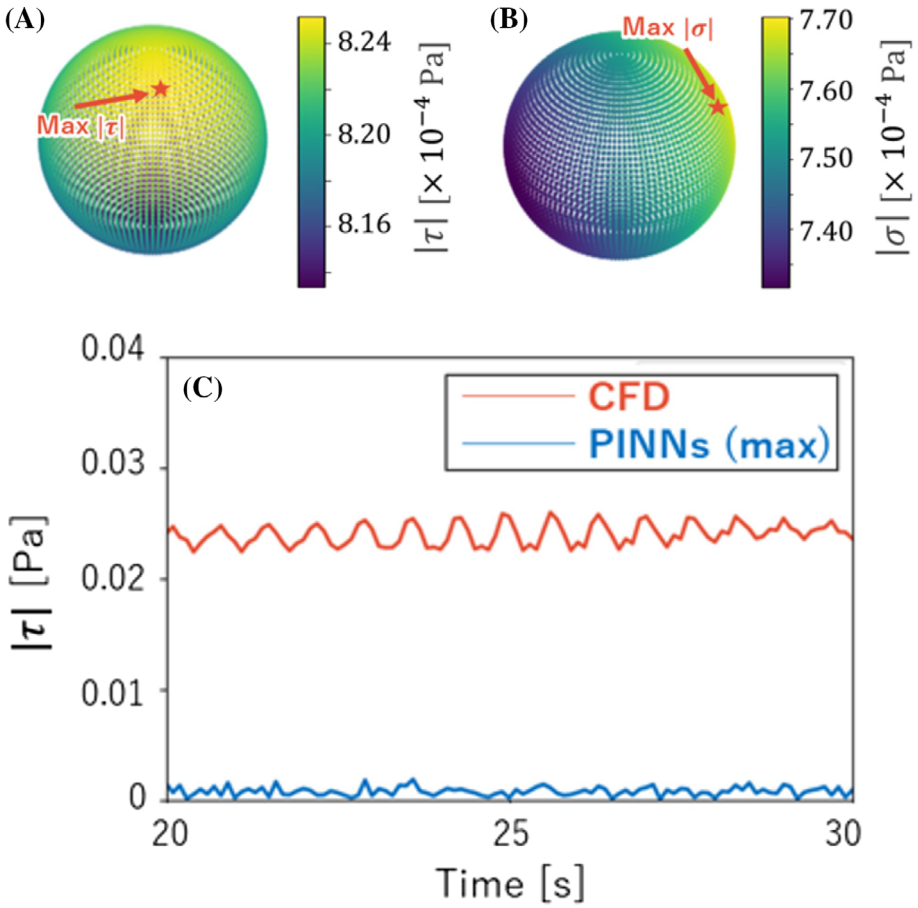

FIGURE 4 Predicted distribution of (A) shear stress and (B) vertical stress, and (C) time profile of shear stress from CFD and PINNs.

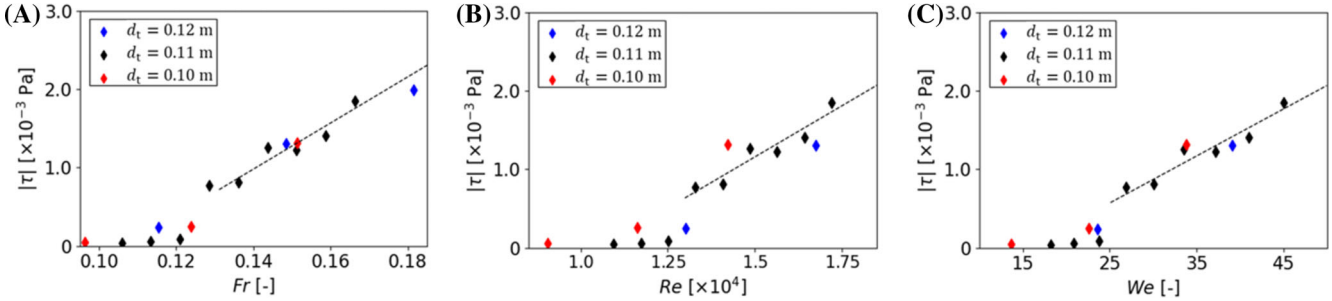

FIGURE 5 Dependency of shear stress on dimensionless numbers, (A) *Fr*, (B) *Re*, and (C) *We*.

of accuracy loss due to rounding error and cancellation. On the other hand, automatic differentiation can calculate partial derivatives without any approximation based on the chain rate of composite functions. Second, particles are smaller than the computational grid. In contrast, PINNs can calculate velocity gradients at arbitrary locations based on training data. The obtained shear stresses can be calculated accurately with definition without approximation. The same applies to vertical stress.

3.3 | Dependence of shear stress on dimensionless numbers

In addition, we evaluated the correlation between the estimated shear stress tau and dimensionless numbers consisting of the dimensionless Navier–Stokes equation (Equation 11). Variables marked with an asterisk mean that they are non-dimensionalised. For conversion into dimensionless equation, the internal diameter of the culture vessel (d_t) was adopted as a characteristic length and velocity of the center of the culture vessel ($R\omega$) was adopted as a characteristic velocity. Definitions of dimensionless numbers were represented in Equations 12–15.

$$\frac{\partial}{\partial t^*}\overline{v_f}^* + \nabla^* \cdot (\overline{v_f}^* \overline{v_f}^*) = -\nabla^* p^* + \frac{1}{Re}\nabla^{*2}\overline{v_f}^* + \frac{1}{Fr^2}e_z - \frac{1}{Dr}a_c^* + \frac{1}{We}\nabla^*\alpha \tag{11}$$

$$Re = \frac{R\omega d_t}{\nu_f} \tag{12}$$

$$Fr = \frac{R\omega}{\sqrt{\nu_f g}} \tag{13}$$

$$Dr = \frac{2R}{d_t} \tag{14}$$

$$We = \frac{\rho_f R^2 \omega^2 d_t}{\gamma} \tag{15}$$

Here, *Re* represents the ratio of inertial force and viscous force of the fluid as a Reynolds' number, *Fr* represents the ratio of inertial force and gravity force of the fluid as a Frude's number, *Dr* represents the ratio of swirling radius and vessel radius, and *We* represents the ratio of inertial force and surface tension of the fluid.

The correlation between $|\tau|$ and these dimensionless numbers (*Fr*, *Re*, and *We*) under fixed *Dr* (=0.273) was evaluated (Figure 5). The shear stress was stable in low dimensionless numbers ($Fr < 0.12$, $Re < 1.25 \times 10^4$, and $We < 25$), and increased linearly over the threshold. This is because cells sedimented into the bottom in the condition of under the threshold, where shear stress was low. On the other hand, in the condition of over the threshold, the number of floating particles increased, and floating particles suffered high shear stress.

4 | CONCLUSION

In this study, PINNs from CFD data were applied to predict the medium flow surrounding cells, which causes shear stress and drag force on the cell surface. The precise estimation of shear stress on cells requires high-resolution data, but obtaining a high-resolution one from CFD requires a fine mesh, which requires high calculation costs and time. In addition, PINNs are expected to apply the shear stress on non-spherical surfaces such as cell aggregates because PINNs do not require mesh preparation. Cells suffer from stress from medium flow during culture operations; therefore, this technique is expected to be used to develop and optimize all culture operations, not only suspension culture.

AUTHOR CONTRIBUTIONS

Ikki Horiguchi: Writing – original draft; writing – review and editing; project administration; supervision; funding acquisition; conceptualization; visualization. **Keisuke Shima:** Methodology; software; data curation; writing – review and editing; conceptualization; investigation; validation; formal analysis; visualization. **Yasunori Okano:** Writing – review and editing; conceptualization; supervision; project administration; resources; validation.

ACKNOWLEDGMENTS

This research was supported by JSPS KAKENHI Grant Number JP23K04507.

DATA AVAILABILITY STATEMENT

The original data and python code for generating Figure 4C are available in Figure 4 directory in the Supporting Information. The plot data and python code for Figure 5 are available in Figure 5 directory in the Supporting Information.

ORCID

Ikki Horiguchi https://orcid.org/0000-0001-6251-6895

REFERENCES

1. Butler M, Meneses-Acosta A. Recent advances in technology supporting biopharmaceutical production from mammalian cells. *Appl Microbiol Biotechnol*. 2012;96(4):885-894. doi:10.1007/s00253-012-4451-z
2. Horiguchi I, Kino-oka M. Current developments in the stable production of human induced pluripotent stem cells. *Engineering*. 2021;7(2):144-152. doi:10.1016/j.eng.2021.01.001
3. Fois CAM, Schindeler A, Valtchev P, Dehghani F. Dynamic flow and shear stress as key parameters for intestinal cells morphology and polarization in an organ-on-a-chip model. *Biomed Microdevices*. 2021;23(4):55. doi:10.1007/s10544-021-00591-y
4. Bertani G, Di Tinco R, Bertoni L, et al. Flow-dependent shear stress affects the biological properties of pericyte-like cells isolated from human dental pulp. *Stem Cell Res Ther*. 2023;14(1):31. doi:10.1186/s13287-023-03254-2
5. Rennier K, Ji JY. The role of death-associated protein kinase (DAPK) in endothelial apoptosis under fluid shear stress. *Life Sci*. 2013;93(5–6):194-200. doi:10.1016/j.lfs.2013.06.011
6. Zhan C, Bidkhori G, Schwarz H, et al. Low shear stress increases recombinant protein production and high shear stress increases apoptosis in human cells. *iScience*. 2020;23(11):101653. doi:10.1016/j.isci.2020.101653
7. Shi J, Wu B, Li S, Song J, Song B, Lu WF. Shear stress analysis and its effects on cell viability and cell proliferation in drop-on-demand bioprinting. *Biomed Phys Eng Express*. 2018;4(4):045028. doi:10.1088/2057-1976/aac946
8. Horiguchi I, Torizal FG, Nagate H, et al. Protection of human induced pluripotent stem cells against shear stress in suspension culture by Bingham plastic fluid. *Biotechnol Prog*. 2021;37(2):1-8. doi:10.1002/btpr.3100
9. Yamamoto K, Takahashi T, Asahara T, et al. Proliferation, differentiation, and tube formation by endothelial progenitor cells in response to shear stress. *J Appl Physiol*. 2003;95(5):2081-2088. doi:10.1152/japplphysiol.00232.2003
10. Horiguchi I, Nagate H, Sakai Y. Particle-tracking-based strategy for the optimization of agitation conditions in a suspension culture of human induced pluripotent stem cells in a shaking vessel. *J Biosci Bioeng*. 2023;135(5):411-416. doi:10.1016/j.jbiosc.2023.02.007
11. Rebej M, Juřena T, Vondál J, Fuente Herraiz D, Červený J, Jegla Z. Numerical simulations and validation of single- and two-phase flow in a stirred lab-scale photobioreactor. *Biosyst Eng*. 2023;230:35-50. doi:10.1016/j.biosystemseng.2023.04.004
12. Lu Z, Wang K, Jin G, Huang K, Huang J. CFD studies on hydrodynamic characteristics of shaking bioreactors with wide conical bottom. *J Chem Technol Biotechnol*. 2018;93(3):810-817. doi:10.1002/jctb.5431
13. Wang L, Okano Y, Horiguchi I, Zhang J. Bayesian optimization for favourable suspension culture of orbitally shaken bioreactors with a hollow cylinder wall. *J Chem Eng Japan*. 2023;56(1):2247046. doi:10.1080/00219592.2023.2247046
14. Morozova N, Trias FX, Capdevila R, Schillaci E, Oliva A. A CFD-based surrogate model for predicting flow parameters in a ventilated room using sensor readings. *Energ Buildings*. 2022;266:112146. doi:10.1016/j.enbuild.2022.112146
15. Raissi M, Perdikaris P, Karniadakis GE. Physics-informed neural networks: a deep learning framework for solving forward and inverse problems involving nonlinear partial differential equations. *J Comput Phys*. 2019;378:686-707. doi:10.1016/j.jcp.2018.10.045
16. Mahmoudabadbozchelou M, Karniadakis GE, Jamali S. Nn-PINNs: non-Newtonian physics-informed neural networks for complex fluid modeling. *Soft Matter*. 2022;18(1):172-185. doi:10.1039/d1sm01298c
17. Qiu R, Huang R, Xiao Y, et al. Physics-informed neural networks for phase-field method in two-phase flow. *Phys Fluids*. 2022;34(5):052109. doi:10.1063/5.0091063
18. Takehara Y, Okano Y, Dost S. Fast prediction of transport structures in the melt by physics informed neural networks during "VMCz" crystal growth of silicon. *J Chem Eng Japan*. 2023;56(1):2236656. doi:10.1080/00219592.2023.2236656
19. Köpf M, Nasehi R, Kreimendahl F, Jockenhoevel S, Fischer H. Bioprinting-associated shear stress and hydrostatic pressure affect the angiogenic potential of human umbilical vein endothelial cells. *Int J Bioprint*. 2022;8(4):96-107. doi:10.18063/ijb.v8i4.606
20. Yano M, Yamamoto T, Okano Y, Kanamori T, Kino-Oka M. Numerical study of fluid dynamics in suspension culture of iPS cells. *Am J Chem Eng*. 2017;1(17):73-81.

SUPPORTING INFORMATION

Additional supporting information can be found online in the Supporting Information section at the end of this article.

How to cite this article: Horiguchi I, Shima K, Okano Y. Physics-informed neural networks (PINNs) for high-resolutional prediction of shear stress on cells in suspension culture. *AIChE J*. 2025;e18853. doi:10.1002/aic.18853